Magnetic Resonance in Medicine 68:543–551 (2012)

Feasibility, Reproducibility, and Reliability for the T_2^* Iron Evaluation at 3 T in Comparison With 1.5 T

Antonella Meloni,[1]* Vincenzo Positano,[1] Petra Keilberg,[1] Daniele De Marchi,[1] Pasquale Pepe,[2] Angelo Zuccarelli,[3] Saveria Campisi,[4] Maria Antonietta Romeo,[5] Tommaso Casini,[6] Pier Paolo Bitti,[7] Calogera Gerardi,[8] Maria Eliana Lai,[9] Basilia Piraino,[10] Gaetano Giuffrida,[11] Giuseppina Secchi,[12] Massimo Midiri,[13] Massimo Lombardi,[1] and Alessia Pepe[1]

This study aimed to determine the feasibility, reproducibility, and reliability of the multiecho T_2^* Magnetic resonance imaging technique at 3 T for myocardial and liver iron burden quantification and the relationship between T_2^* values at 3 and 1.5 T. Thirty-eight transfusion-dependent patients and 20 healthy subjects were studied. Cardiac segmental and global T_2^* values were calculated after developing a correction map to compensate the artifactual T_2^* variations. The hepatic T_2^* value was determined over a region of interest. The intraoperator and interoperator reproducibility for T_2^* measurements at 3 T was good. A linear relationship was found between patients' R_2 (1000/T_2^*) values at 3 and 1.5 T. Segmental correction factors were significantly higher at 3 T. A conversion formula returning T_2^* values at 1.5 T from values at 3 T was proposed. A good diagnostic reliability for T_2^* assessment at 3 T was demonstrated. Lower limits of normal for 3 T T_2^* values were 23.3 ms, 21.1 ms, and 11.7 ms, for the global heart, mid-ventricular septum, and liver, respectively. In conclusion, T_2^* quantification of iron burden in the mid-ventricular septum, global heart, and no heavy–moderate livers resulted to be feasible, reproducible, and reliable at 3 T. Segmental heart T_2^* analysis at 3 T may be challenging due to significantly higher susceptibility artifacts. Magn Reson Med 68:543–551, 2012. © 2011 Wiley Periodicals, Inc.

[1]CMR Unit, Fondazione G.Monasterio CNR-Regione Toscana and Institute of Clinical Physiology, Pisa, Italy

[2]Epidemiology and Biostatistics Unit, Institute of Clinical Physiology, CNR, Pisa, Italy

[3]Centro trasfusionale e di microcitemia, Ospedale civile, Olbia, Italy

[4]U.O.S. Talassemia, A.O. Umberto I, Siracusa, Italy

[5]Dipartimento Pediatria, Azienda Policlinico, Catania, Italy

[6]Centro Talassemie ed Emoglobinopatie, Ospedale Meyer, Firenze, Italy

[7]Servizio Immunoematologia e Medicina Trasfusionale, Dipartimento dei Servizi, P. O. San Francesco, Nuoro, Italy

[8]Unità Operativa Semplice di Talassemia, P.O. "Giovanni Paolo II", Sciacca Distretto AG2- ASP Agrigento, Sciacca (AG), Italy

[9]Centro Talassemici Adulti, Ospedale microcitemico, Cagliari, Italy

[10]U.O. Genetica e Immunologia Pediatrica, Policlinico "G. Martino", Messina, Italy

[11]Divisione Clinicizzata di Ematologia, Ospedale "Ferrarotto", Catania, Italy

[12]Servizio trasfusionale, Azienda USL n 1, Sassari, Italy

[13]Department of Radiology, University of Palermo, Palermo, Italy

Grant sponsors: Ministero della Salute, fondi ex art. 12 D.Lgs. 502/92 e s.m.i., ricerca sanitaria finalizzata anno 2006, and Fondazione L. Giambrone

*Correspondence to: Antonella Meloni, Ph.D., CMR Unit, Fondazione G. Monasterio CNR-Regione Toscana and Institute of Clinical Physiology, Via Moruzzi, 1-56124 Pisa, Italy. E-mail: antonella.meloni@ifc.cnr.it

Received 29 June 2011; revised 6 September 2011; accepted 6 September 2011.

DOI 10.1002/mrm.23236

Published online 29 November 2011 in Wiley Online Library (wileyonlinelibrary.com).

Key words: iron overload; T_2^* magnetic resonance; 3 T; heart; liver

Patients with anemia often need regular blood transfusions, which can cause an increased iron accumulation in a variety of organs (1). Thus, these patients are subjected to a chelation therapy (2) and a direct monitoring of the treatment's efficacy is strongly needed (3). The T_2^* Magnetic Resonance Imaging (MRI) technique is the most robust method for the noninvasive quantification of cardiac and hepatic iron overload (4,5). This indirect method has been validated on 1.5 T MRI scanners (6,7), generally used in the clinical arena. However, there is an increasing number of centers using 3 T MRI scanners. As T_2^* values decrease with increasing field strength (8–10), at 3 T the connections T_2^*-iron overload must be redefined and proper cut-offs must be introduced. Two works have addressed this issue in human subjects (11,12). T_2^* measurement was performed only in the mid-septum. Recently, a multislice T_2^* approach has been validated at 1.5 T as technique for the evaluation of segmental myocardial iron distribution (13–15).

Thus, the goals of this study were to evaluate the feasibility, the intraobserver and interobserver variability and the reliability of the multislice multiecho T_2^* approach at 3 T, to determine the relationship between T_2^* values at 3 and 1.5 T for heart and liver over a moderate-sized study cohort and to determine the lower limits of normal for heart and liver at 3 T.

MATERIALS AND METHODS

Study Population

Thirty-eight transfusion-dependent patients (22 men and 16 women, mean age 35.7 ± 7.5 years) enroled in the Myocardial Iron Overload in Thalassemia (MIOT) Network (16) were scanned at 1.5 and 3 T on the same day.

Moreover, 20 healthy subjects (9 men and 11 women, mean age 33.5 ± 4.1 years) underwent MRI at 3 T.

The control group was not statistically different from the study population for age and sex ($P = 0.160$ and 0.832, respectively).

The study complied with the Declaration of Helsinki. All subjects gave written informed consent to the study.

MRI

GE systems (Signa CVi 1.5 T and Signa HDx 3 T; GE Healthcare, Waukesha, WI) were used. A four-element and an eight-element cardiac phased-array receiver

surface coil were used for signal reception at 1.5 T and 3 T scanners, respectively.

For myocardial iron overload assessment, three parallel short-axis views (basal, medium, and apical) of the left ventricle were obtained by a T_2^* gradient-echo multiecho sequence with electrocardiogram triggering (13). Each slice (thickness 8 mm) was acquired at 10 echo times (TEs; 1.5 T: TEs 2.0–21.8 ms, $\Delta TE = 2.20$ ms; 3 T: TEs 1.64–20.2 ms, $\Delta TE = 2.06$ ms) in a single end-expiratory breath-hold. A matrix of 192 × 192 pixels and a bandwidth of ±83.3 kHz were used with 12–16 views per segment depending on heart rate. The flip angle was 25° at 1.5 T and 20° at 3 T, the repetition time was 23.9 ms at 1.5 T and 22.4 ms at 3 T, while a field of view 40 × 40 cm and 35 × 35 cm was used at 1.5 T and 3 T, respectively. Acquisition time for each slice ranged from 10 to 18 s depending on heart rate.

For liver iron overload assessment, a T_2^* gradient-echo multiecho sequence was used (17). A medium-hepatic slice (thickness 8 mm) was obtained at 10 TEs (1.5 T: TEs 2.0–20.9 ms, $\Delta TE = 2.1$ ms; 3 T: first TE 1.45 ms, $\Delta TE = 2.2$ ms). A matrix of 192 × 192 pixels, a bandwidth of 83.3 kHz, and a repetition time of 34 ms were used. The flip angle was 25° at 1.5 T and 20° at 3 T, while a field of view 40 × 40 cm and 35 × 35 cm was used at 1.5 T and 3 T, respectively. The mean scan time was 8 s.

Image Analysis

Acquired images were analyzed using a custom-written software, previously validated and now commercially available (Hippo-MIOT®, Ref. 14).

The myocardium was divided into 16 segments, according to the American Heart Association/American College of Cardiology standardized model (18), and the T_2^* value in each segment was obtained. In particular, the mean value of the signal intensity along all TE values was calculated for each segment, and the assessed decay curve was fitted to a monoexponential model. Manual truncation was applied to discard the late TEs with low signal-to-noise ratio. Moreover, the software provided the global heart T_2^* value averaged over all segmental values and the T_2^* value in the mid-ventricular septum, obtained by averaging T_2^* values in segments eight and nine. The reproducibility of this methodology at 1.5 T had been previously assessed (7,19).

For the liver, the decay curve was extracted from a region of interest of standard dimension (area of 90 pixels) drawn by the operator avoiding the blood vessels, and the T_2^* value was calculated by fitting the decay curve to a single exponential with a constant offset model (20). Care was taken to avoid placement of the region of interest in the posterior lateral (VII) and medial (VIII) segments, more prone to susceptibility artifacts (17).

Artifacts Map at 3 T

Because segmental T_2^* assessment in heart can be affected by susceptibility artifacts (21), a susceptibility artifacts map at 1.5 T has been previously developed (14). This map was implemented in the software and used to normalize segmental data. The artifacts effect is expected to be different at 3 T, so a map for the correction of artifactual T_2^* fluctuations at 3 T was built using the same approach.

The map was developed in the R_2^* ($1000/T_2^*$) domain using the healthy subjects data. The segmental correction factor for each segment was defined as the sum of the averaged deviations of the R_2^* in the segment with respect to the global R_2^* value plus a constant factor representing the global drift in R_2^* measurement. To evaluate the drift, the artifacts were assumed minimal in the mid-ventricular septum. So, the correction factors were normalized with respect to the mid-ventricular septum value.

Corrected T_2^* values were evaluated by transforming T_2^* values in the corresponding R_2^* ones, subtracting the corresponding artifacts map values, and returning to T_2^* notation.

Intraobserver and Interobserver Variability Assessment of 3 T T_2^* Values

Data related to 20 patients (3 T) were randomly selected from the entire data set. To evaluate the intraobserver variability, the selected images were blindly reanalyzed by the same observer after 2 weeks. To evaluate the interobserver variability, all the selected images were presented in random order to another operator, who did not know the results obtained by the other one. The analysis was redone by the observers starting border drawing for the heart and with region of interest placement for the liver.

Relationship Between T_2^* Values at 3 and 1.5 T

The R_2^* is directly proportional to tissues iron concentration (22), so the R_2^* values at 1.5 and 3 T can be expressed as:

$$R^*_{21.5\,\mathrm{T}} = k_{1.5\,\mathrm{T}} C_{\mathrm{Fe}} + R^*_{2t1.5\,\mathrm{T}} \qquad R^*_{23\,\mathrm{T}} = k_{3\,\mathrm{T}} C_{\mathrm{Fe}} + R^*_{2t3\,\mathrm{T}} \quad [1]$$

$R^*_{2t15\ \mathrm{T}}$ and $R^*_{2\ t3\ \mathrm{T}}$ represent the R_2^* values of the imaged tissue without iron overload, C_{Fe} represents the tissue iron concentration, $k_{3\ \mathrm{T}}$ and $k_{1.5\ \mathrm{T}}$ depend on the static magnetic field strength and other factors (8). Consequently, the relationship between R_2^* values at 3 and 1.5 T is linear:

$$R^*_{23\,\mathrm{T}} = \frac{k_{3\,\mathrm{T}}}{k_{1.5\,\mathrm{T}}} R^*_{21.5\,\mathrm{T}} + \left(R^*_{2_{t3\,\mathrm{T}}} - \frac{k_{3\,\mathrm{T}}}{k_{1.5\,\mathrm{T}}} R^*_{2t1.5\,\mathrm{T}} \right) \quad [2]$$

The Eq. 2 can be simplified as:

$$R^*_{23\,\mathrm{T}} = aR^*_{21.5\,\mathrm{T}} + I. \quad [3]$$

Hence, it is more straightforward to detect the relationship in terms of R_2^* values. The R_2^* values at 3 T were plotted versus the correspondent values at 1.5 T. Data were fitted to a straight line, of which the slope (a) and the y-intercept (I) were extracted, as well as the R^2 value, measuring the reliability of the linear relationship.

In the clinical practice, it is most common to use T_2^* values. T_2^* values at 3 T can be computed as a function of 1.5 T values by inverting the members of the Eq. 3:

$$T^*_{23\,\mathrm{T}} = \frac{1000}{\frac{1000a}{T^*_{21.5\,\mathrm{T}}} + I} \quad [4]$$

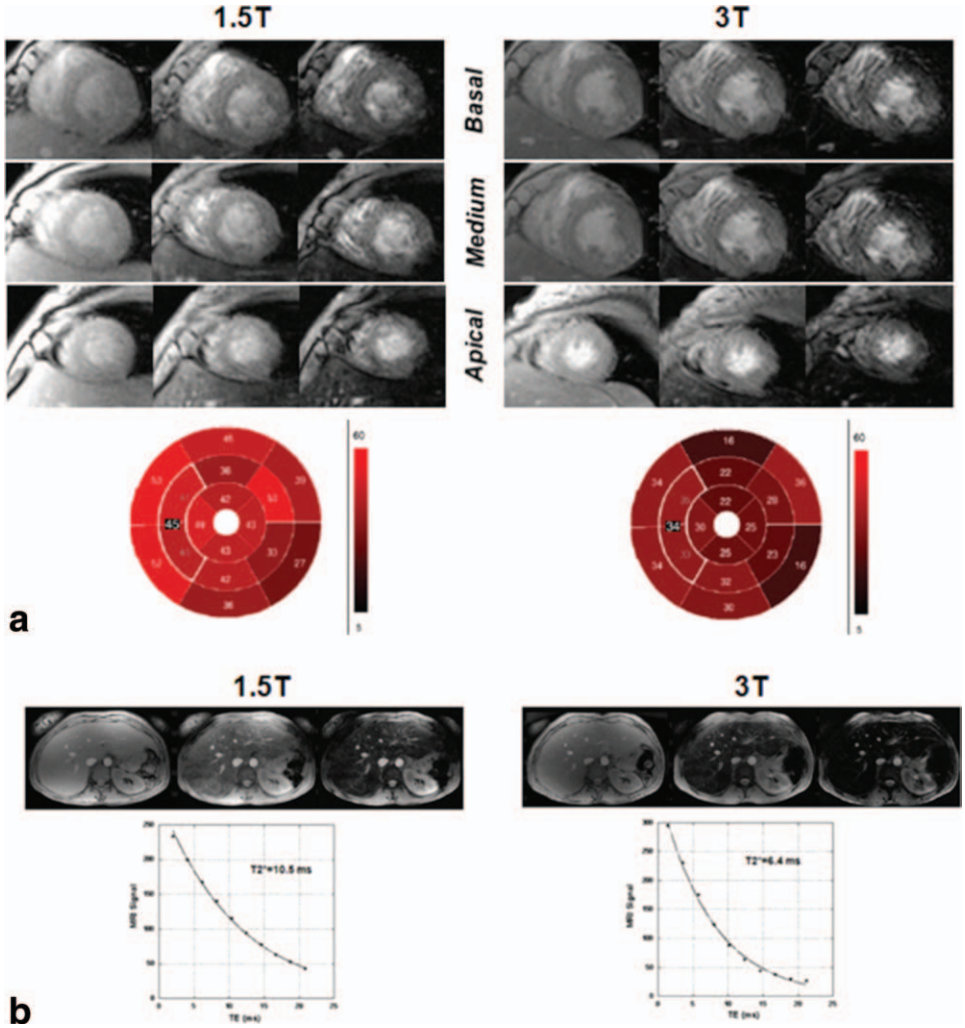

FIG. 1. **a:** Cardiac slices (basal, medium, and apical) at the first, fifth, and last TEs at 1.5 T (left) and 3 T (right) in a thalassemia intermedia patient with normal heart T_2^* segmental values. The two corresponding bull's eyes are shown below. **b:** Liver images at the first, fifth, and last TEs and the corresponding decay curves at 1.5 T (left) and 3 T (right) in the same thalassemia intermedia patient as in (a).

The need is to convert the nonconventional T_2^* values at 3 T into the corresponding T_2^* values at 1.5 T. A general conversion formula can be extracted by the Eq. 4:

$$T^*_{21.5\ \mathrm{T}} = \frac{1000a}{\frac{1000}{T^*_{23\ \mathrm{T}}} - I} \qquad [5]$$

Assessment of Reliability of MRI Findings at 3 T

The "conservative" value of 20 ms is commonly used as the lower limit of normal for the segmental, global heart, and mid-ventricular septum T_2^* values at 1.5 T (14,23,24). Using Eq. 4, a correspondent threshold for T_2^* measurements at 3 T was extracted.

Moreover, the T_2^* threshold values commonly used in management of thalassemia major patients for the liver (22,25) were converted at 3 T (Table 3).

The categorization in normal and pathological T_2^* values performed at 1.5 T was considered as the standard of reference. So, it was detected, if the T_2^* classifications at 3 T were true positive, false positive, true negative, and false negative. Sensitivity, specificity, positive and negative predictive values and accuracy were also calculated.

Statistical Analysis

All data were analyzed using SPSS and MedCalc statistical packages.

In the reproducibility assessment, the difference between two analyses was evaluated by calculating the coefficient of variation and the interclass correlation coefficient (ICC). The coefficient of variation was calculated as the ratio of the standard deviation (SD) of the half mean square of the differences between the repeated values to the general mean. The ICC was obtained from a two-way random effects model with measures of absolute agreement. An ICC $\geq$ 0.75 was considered excellent, between 0.40 and 0.75 good, and $<$0.40 unsatisfactory.

The relationship between global heart and mid-ventricular septum T_2^* was assessed using the Spearman correlation coefficient.

To compare the original T_2^* values at 1.5 T with the T_2^* values calculated by Eq. 5, the Wilcoxon's signed rank test, the Spearman correlation coefficient, and the ICC were considered. Summary data were displayed using scatter plots with regression lines and Bland–Altman plots.

The lower limit of normal for the T_2^* value was calculated on log-transformed and consequently normalized data of healthy subjects as mean minus 2 * SD.

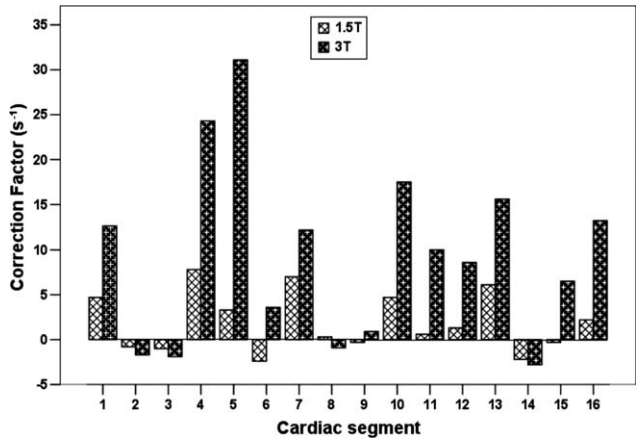

FIG. 2. Comparison between segmental correction factors at 3 T detected using the data of healthy subjects involved in this study and segmental correction factor at 1.5 already implemented in the Hippo MIOT IFC-CNR® Software.

$P < 0.05$ was considered statistically significant.

RESULTS

Feasibility of Multislice Approach at 3 T

Multislice T_2^* imaging at 3 T was feasible in all subjects, and all images were successfully analyzed. Figure 1a shows the heart short-axis slices at 1.5 and 3 T and the two corresponding bull's eye representations of the 16 T_2^* segmental values.

Segmental Correction Factors

Figure 2 shows the segmental correction factors found in this study for 3 T images and those used for images at 1.5 T, detected in a previous study (14). The correction factors globally considered were significantly higher at 3 T ($P = 0.002$). In particular, the correction factors were significantly higher at 3 T in all segments with the exception of the septum.

Intraobserver and Interobserver Variability at 3 T

The results of the intraobserver and interobserver variability analysis performed in the selected 3 T images are summarized in Table 1.

Patients Findings

The global heart and the mid-ventricular septum T_2^* values averaged in the whole patient population were, respectively, 30.8 ± 11.3 ms and 33.5 ± 13.2 ms at 1.5 T, whereas 27.6 ± 11.8 ms and 25.2 ± 10.9 ms at 3 T. At both field strength the mid-ventricular septum and the global heart, T_2^* values were significantly correlated (1.5 T: $r = 0.949$, $P < 0.0001$; 3 T: $r = 0.953$, $P < 0.0001$). For the global heart R_2^*, the best-fitting line had a slope of 1.945 ± 0.055 and an intercept of −24.806 ± 3.304 s^{-1} ($R^2 = 0.972$; Fig. 3a). For the mid-ventricular septum, R_2^* values the best-fitting line had a slope of 2.180 ± 0.097 and an intercept of −23.292 ± 5.549 s^{-1} ($R^2 = 0.934$; Fig. 3b). The linear fit was performed even for the segmental T_2^* values, finding a slope of 2.003 ± 0.044 and an intercept of −26.054 ± 2.820 s^{-1} ($R^2 = 0.779$).

Figure 1b shows liver images and the two corresponding signal decay curves extracted from the defined region of interests at 1.5 and 3 T from the same patient in Fig. 1a. In the whole patient population, the mean liver T_2^* value was 9.0 ± 7.2 ms at 1.5 T and 5.4 ± 4.6 at 3 T. At very high iron tissue concentrations, the T_2^* assessment lacks of precision because of the inadequate minimum TE (26), so the patients with an R_2^* value at 1.5 T greater than 1000 s^{-1} were excluded from the fit (cross-shaped markers in Fig. 4). The best-fitting line had a slope of 1.917 ± 0.061 and an intercept of −9.145 ± 13.083 s^{-1} ($R^2 = 0.973$).

Conversion of T_2^* Values at 3 T to T_2^* Values at 1.5 T

Table 2 shows the T_2^* values at 1.5 T obtained by Eq. 5 using the slopes and the intercepts detected. The extracted global heart T_2^* values (30.1 ± 10.4 ms) were

Table 1
Intraobserver and Interobserver Reproducibility Data for T_2^* Values at 3 T

	Intraobserver reproducibility		Interobserver reproducibility	
	ICC	CoV (%)	ICC	CoV (%)
Global heart	0.998	2.53	0.995	3.62
Mid-ventricular septum	0.994	4.85	0.988	6.62
Segment basal anterior	0.957	12.91	0.931	15.67
Segment basal anteroseptal	0.994	5.04	0.986	7.27
Segment basal inferoseptal	0.989	6.47	0.977	8.82
Segment basal inferior	0.971	10.23	0.931	15.57
Segment basal inferolateral	0.958	11.79	0.899	16.92
Segment basal anterolateral	0.962	11.84	0.935	14.69
Segment medium anterior	0.977	9.70	0.973	10.07
Segment medium anteroseptal	0.988	6.98	0.980	9.27
Segment medium inferoseptal	0.986	7.10	0.991	5.33
Segment medium inferior	0.950	13.43	0.929	16.52
Segment medium inferolateral	0.964	10.84	0.981	7.97
Segment medium anterolateral	0.991	5.69	0.970	9.99
Segment apical anterior	0.976	10.25	0.965	12.33
Segment apical septal	0.996	4.05	0.970	11.11
Segment apical inferior	0.978	9.43	0.989	6.72
Segment apical lateral	0.994	4.77	0.983	8.14
All segments	0.979	8.94	0.965	11.39
Liver	0.999	4.69	0.998	6.17

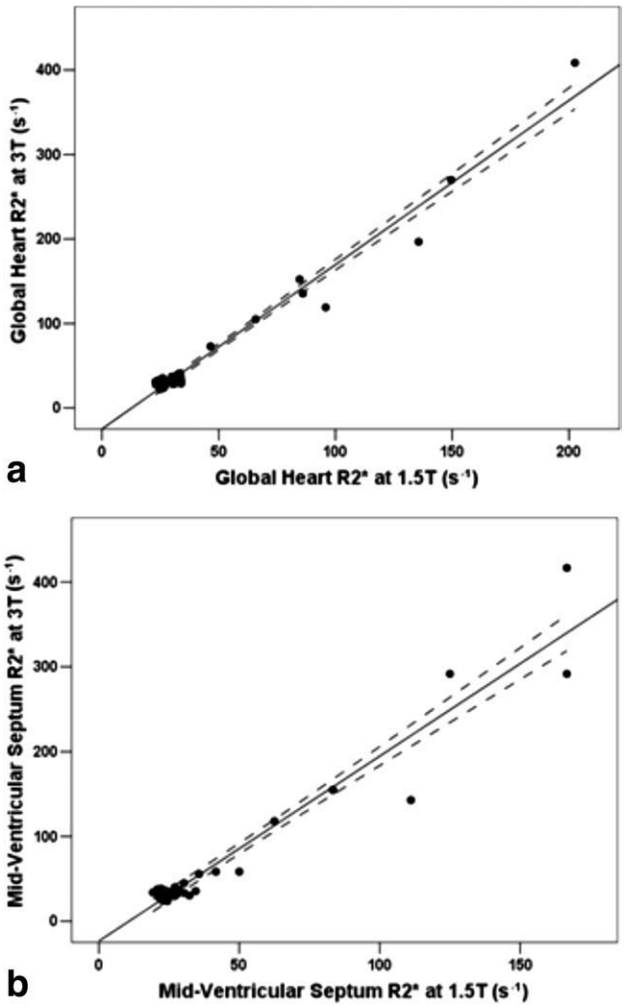

FIG. 3. Global heart (**a**) and mid-ventricular septum (**b**). R_2^* values at 3 T versus the corresponding R_2^* values at 1.5 T for transfusion-dependent patients. The line of best fit and the curves indicating 95% confidence interval (CI) are indicated.

not significantly different from the original T_2^* values at 1.5 T ($P = 0.491$; Fig. 5a). The best-fitting line had a slope of 0.871 ± 0.049 and an intercept of 3.317 ± 1.597 ms ($R^2 = 0.898$). The correlation between the values was significant ($r = 0.774$, $P < 0.0001$), and an ICC of 0.971 was found. For the mid-ventricular septum, the extracted T_2^* values were not significantly different from the original values ($P = 0.528$). The best-fitting line had a slope of 0.852 ± 0.1506 and an intercept of 5.680 ± 2.021 ms ($R^2 = 0.853$; Fig. 5c). The correlation between the values was significant ($r = 0.709$, $P < 0.0001$), and an ICC of 0.957 was found. The Bland–Altman analysis is shown in Fig. 5b,d.

For the liver, the extracted T_2^* values (9.6 ± 7.7 ms) were not significantly different from the original T_2^* values at 1.5 T ($P = 0.118$; Fig. 6a). The best-fitting line had a slope of 1.046 ± 0.045 and an intercept of 0.115 ± 0.518 ms ($R^2 = 0.944$). The correlation between the values was significant ($r = 0.983$, $P < 0.0001$), and an ICC of 0.983 was found. The Bland–Altman analysis is presented in Fig. 6b.

Diagnostic Reliability at 3 T

Using Eq. 4, the lower limit of normal of 20 ms for the heart corresponded to 13.8 ms at 3 T. Table 4 shows the efficacy of 3 T MRI in differentiating normal from pathological T_2^* values. The sensitivity was under 80% for three myocardial segments, whereas specificity was always very strong (high 90's). The accuracy was very high (high 90's) and dropped always for one segment. The mid-ventricular septum T_2^* value was always correctly classified. One false positive was found in the global heart T_2^* values classification dropping the positive predictive value. The global heart T_2^* values for the patient misdiagnosed were 21.5 ms at 1.5 T and 13.7 ms at 3 T, very close to the cut-off.

Table 4 shows the efficacy of 3 T MRI in classifying patients with different levels of liver iron burden. The accuracy was high to identify patients with mild to no liver iron burden. To identify patients with heavy and moderate liver iron burden, the accuracy dropped to 94% with an unsatisfactory sensitivity to detect patients with heavy liver iron burden.

Lower Limits of Normal

Global heart T_2^* values at 3 T ranged from 21.6 to 28.0 ms, with a mean of 23.6 and a SD of 1.9 ms. The lower limit of normal was 20 ms.

The mid-ventricular septum T_2^* values at 3 T ranged from 20.4 to 32.8 ms, with a mean of 27.9 and a SD of 3.5 ms. The lower limit of normal was 21.1 ms.

Liver T_2^* values at 3 T ranged from 11.0 to 26.9 ms, with a mean of 18.9 and a SD of 4.2 ms. The lower limit of normal was 11.6 ms.

DISCUSSION

Three-tesla scanners have been installed widely, and an increasing number of sites have only 3-T scanners, in particular in geographic areas (i.e., Asia) where the

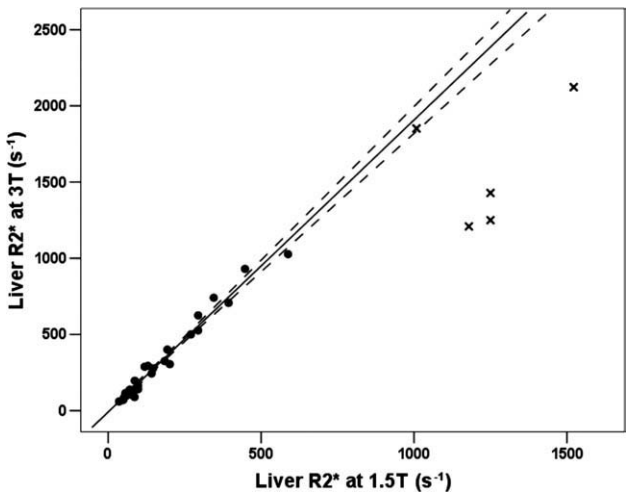

FIG. 4. Liver R_2^* values at 3 T versus liver R_2^* values at 1.5 T for transfusion-dependent patients. The line the line of best fit and the curves indicating 95% CI are indicated. The cross-shaped markers indicate the patients excluded from the best-fit analysis.

Table 2
T_2^* Values at 1.5 T Evaluated Starting by the T_2^* at 3.0 T by Means of the Eq. 4

Original T_2^* values at 3 T (ms)	T_2^* values at 1.5 T evaluated with the Eq. 6 (ms)		
	Global Heart $T^*_{21.5\ T} = \frac{1945}{\frac{1000}{T^*_{2\ 3\ T}} + 24.806}$	Mid-ventricular septum $T^*_{21.5\ T} = \frac{2180}{\frac{1000}{T^*_{23\ T}} + 23.292}$	Liver $T^*_{21.5\ T} = \frac{1917}{\frac{1000}{T^*_{23\ T}} + 9.145}$
1	1.90	2.13	1.95
1.5	2.84	3.16	2.92
2	3.77	4.17	3.87
2.5	4.69	5.15	4.82
3	5.60	6.11	5.76
3.5	6.50	7.05	6.68
4	7.40	7.98	7.61
4.5	8.29	8.88	8.52
5	9.17	9.76	9.42
5.5	10.04	10.63	10.32
6	10.90	11.48	11.21
6.5	11.76	12.31	12.09
7	12.61	13.12	12.97
7.5	13.45	13.92	13.83
8	14.29	14.70	14.69
8.5	15.12	15.47	15.55
9	15.94	16.22	16.39
9.5	16.76	16.96	17.23
10	17.56	17.68	18.06
11	19.16	19.09	19.70
12	20.73	20.45	21.31
13	22.27	21.75	22.90
14	23.79	23.02	24.46
15	25.29	24.23	26.00
16	26.76	25.41	27.51
17	28.20	26.55	29.00
18	29.63	27.65	30.46
19	31.03	28.71	31.91
20	32.41	29.74	33.32
22	35.11	31.71	36.10
24	37.73	33.56	38.79
26	40.27	35.30	41.40
28	42.73	36.95	43.94
30	45.13	38.50	46.40

For each district (global heart, mid-ventricular septum, and liver), the equation with the corresponding values used for the slope and the intercept is indicated.

prevalence of iron-loaded anemia is high and the availability of MRI scans to quantify iron burden is low. Thus, there is the need to assess the feasibility, the intraobserver and interobserver variability, and the reliability of T_2^* measurements at 3 T.

The intraoperator and interoperator reproducibility for T_2^* measurements at 3 T were very good (Table 1) and comparable with those previously found for T_2^* measurements at 1.5 T (7). As expected, the coefficient of variation for the global heart T_2^* was the smallest, due to a "compensation" of outliers that may lead to high variability in a single segment measurement. The variability of T_2^* measurements at 3 T has never been investigated and a proved low intraobserver and interobserver variability is vital for follow-up and research purposes.

Our study confirmed the feasibility of T_2^* measurements at 3 T previously documented (11,12,27). However, some technical issues remain problematic for high-field T_2^*, such as the correction of susceptibility artifacts. Advanced fat–water imaging methods may provide simultaneous, unconfounded estimates of water, fat, T_2^*, and B_o field maps (28). Using the B_o field maps, T_2^* values corrected for macroscopic susceptibility can be obtained. However, when fat–water imaging is not available and only the correction of segmental T_2^* values is needed, a simpler procedure could be adopted, as previously made at 1.5 T (14). In this study, a segmental correction map at 3 T was developed. Thus, we quantified the higher prevalence of susceptibility artifacts at higher fields that seemed to spare only the septal regions.

The advantage of 3 T in terms of improved signal-to-noise ratio was not evident in this study, due to the segmental measurement adopted. T_2^* mapping with a pixel-by-pixel curve fitting may be significantly better at 3 T.

The most correct way to assess the relationship between T_2^* values at 3 T and iron load is calibration against biopsy. However, the biopsies are invasive and no highly sensitive due to the heterogeneous iron deposition in heart and liver (29,30). Also, autoptic studies are challenge due to the low availability. So, we performed an indirect calibration against 1.5 T values, for which the relationship with tissue iron concentration has been established in the liver (22) and in the gerbil hearts (31). In human subjects, an attempt to study the relationship 3 T/1.5 T in the R_2^* space was done by Storey et al. (11) in a relatively small patient cohort ($N = 14$), so in the fitting operation patients and control, subjects were considered as a unique group. R_2^* values at 3 T were about twice that at 1.5 T in both mid-ventricular septum and liver (1.88 and 2.00, respectively). Slope values in our study were 1.945, 2.180, and 1.917 for global heart, mid-ventricular septum, and liver, respectively, quite consistent with the Storey's study and the theoretical model. The twofold increase of R_2^* is also in agreement with the results obtained in the iron-loaded liver synthetic model developed by Ghugre et al. (32). The intercepts were negative and strongly different between heart and liver due to the different matrix of the tissue. The concordance between global and mid-ventricular septum values confirmed the consistence of measurements. Guo et al. (12) performed a linear fitting in T_2^* space in the mid-ventricular septum at 3 and 1.5 T on 18 patients, making a direct comparison not possible.

In the clinical setting, T_2^* values at 1.5 T are generally adopted so a conversion formula between T_2^* values at 3

Table 3
Reference Ranges Used to Evaluate the Severity of the Hepatic Iron Loading With the Cut-off T_2^* Values at Both 1.5 and 3 T

Level of liver iron accumulation	LIC (mg/g/dw)	T_2^* at 1.5 T (ms)	T_2^* at 3 T (ms)
Borderline	<3	9.2–18	5.0–10.3
Mild	3–6.9	9.1–3.9	4.9–2.1
Moderate	7–14	3.8–1.8	2.0–0.95
Heavy	>14	<1.8	<0.95

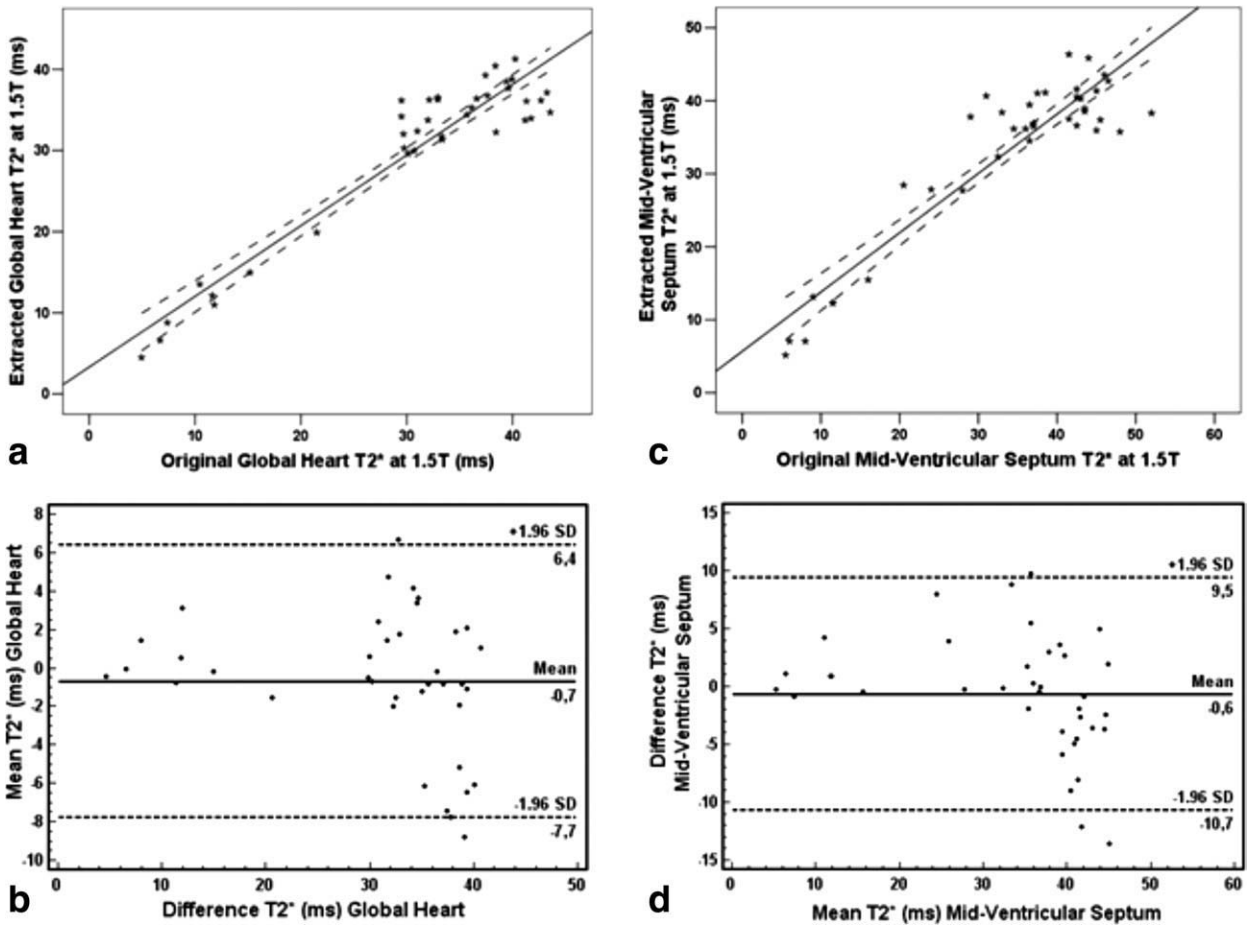

FIG. 5. Comparison between extracted and original T_2^* values at 1.5 T for both global heart and mid-ventricular septum. Scatter plot with linear regression for (**a**) global heart and (**c**) mid-ventricular septum data. Bland–Altman plot of absolute differences for (**b**) global heart and (**d**) mid-ventricular septum data. Dotted lines show 95% CIs.

Table 4
Sensitivity, Specificity, Positive and Negative Predictive Values, and Accuracy for the Segmental, Global Heart, Mid-Ventricular Septum, and Liver T_2^* Assessments at 3 T

	Sensitivity (%)	Specificity (%)	Positive predictive value (%)	Negative predictive value (%)	Accuracy (%)
Heart					
Segment basal anterior	78	96	88	93	92
Segment basal anteroseptal	100	97	88	100	97
Segment basal inferoseptal	100	94	75	100	95
Segment basal inferior	88	96	88	96	94
Segment basal inferolateral	50	100	100	84	86
Segment basal anterolateral	89	100	100	97	97
Segment medium anterior	78	100	100	94	95
Segment medium anteroseptal	88	97	88	97	95
Segment medium inferoseptal	100	97	88	100	97
Segment medium inferior	100	97	89	100	97
Segment medium inferolateral	78	97	88	93	92
Segment medium anterolateral	88	100	100	97	97
Segment apical anterior	100	100	100	100	100
Segment apical septal	100	97	89	100	97
Segment apical inferior	100	97	89	100	97
Segment apical lateral	100	97	88	100	97
Global heart	100	97	88	100	97
Mid-ventricular septum	100	100	100	100	100
Liver					
No iron	100	97	80	100	97
Borderline	91	100	100	96	97
Mild	100	96	88	100	97
Moderate	83	93	83	96	94
Heavy	67	100	100	93	94

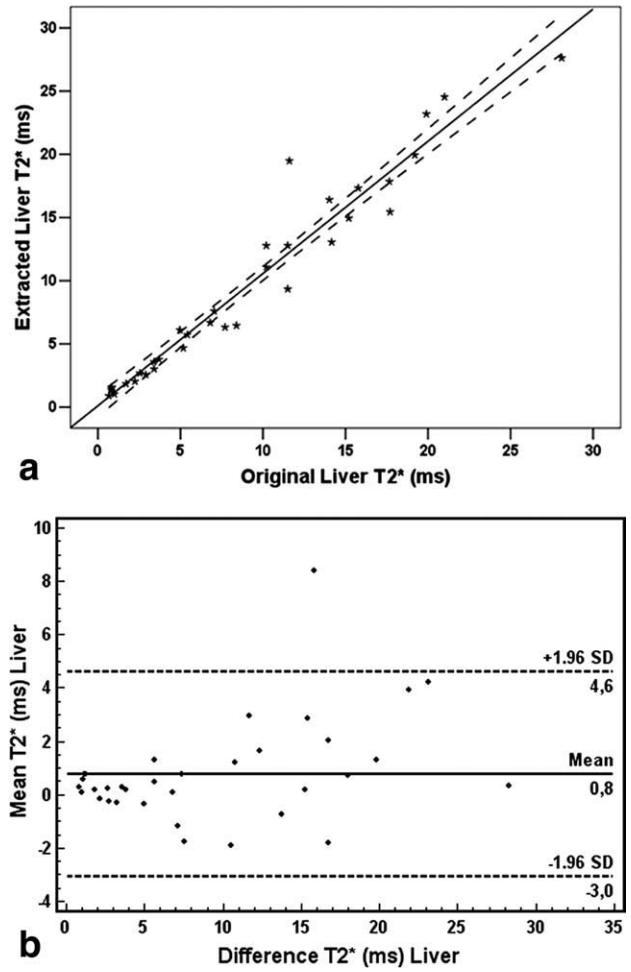

FIG. 6. Comparison between extracted and original liver T_2^* values at 1.5 T. **a:** Scatter plot with linear regression. **b:** Bland–Altman plot of absolute differences. Dotted lines show 95% CIs.

and 1.5 T was proposed (Table 2). Greater differences between extracted and original T_2^* values were detected for high T_2^* values (Figs. 5b,d and 6b), for which measures' precision is low, due to technical constraints in sequence design (26,33).

At 3 T, we found a full diagnostic reliability to evaluate myocardial iron burden in the mid-ventricular septum (Table 4) reflecting the nonsignificant difference in the susceptibility artifacts in this region at 1.5 and 3 T. Also for the global heart T_2^* value, the diagnostic reliability was high after the application of an appropriate correction procedure. For the segmental measurement of iron levels at 3 T, the accuracy was no optimal, reflecting the significant difference in the susceptibility artifacts at 1.5 and 3 T. The accuracy was high to identify patients with mild to no liver iron burden (97%) but dropped to 94% in the identification of patients with heavy–moderate liver iron burden. The sensitivity was unsatisfactory (67%) to detect patients with heavy liver iron burden.

Lower limits of normal at 3 T may seem slightly higher than that found during the validation of the MIOT network (7). The last TE used in the acquisition sequence was about 20 ms both at 3 T and at 1.5 T. Ideally, the longest TE would be approximately twofold longer than the longest T_2^* (26). Consequently, only a part of the signal decay was sampled in not iron-overloaded tissues. It may be expected that the problem will be less important at 3 T, where the mean T_2^* value in normal tissue decreases. It may explain the lower SD value assessed at 3 T and the consequent higher lower limit of normal.

The first limitation of our study was that the cardiac T_2^* values were not well distributed, although it covers the range of clinically relevant T_2^* values, and a strong imbalance toward higher values was present. In fact, for the 1602 patients enroled in the MIOT network, the mean global heart T_2^* value at the first MRI at 1.5 T was 30.0 $\pm$ 21.7 ms, suggesting that our population is generally not iron overloaded, probably due to efficient and well-tailored chelation regimens. This is evident even in Fig. 3a. Thirty patients (79%) had a global heart R_2^* at 1.5 between 22.9 and 33.9 s^{-1} (T_2^* between 29.5 and 43.6 ms). The scale of the *X*-axis is very large (0–200 s^{-1}), so a sort of cluster seems to be present in the image in correspondence to a R_2^* value at 1.5 T of 28.5 s^{-1}. The high prevalence of no iron-loaded patients in our study population could have negatively influenced the diagnostic reliability. The second limitation was that in the fitting operation for the liver R_2^* values at 3 T versus 1.5 T, we excluded five patients because of the very higher R_2^* value. T_2^* multiecho sequences used in clinical practice assure an acceptable precision for T_2^* values greater than 2 ms or less, depending on the used hardware (33). For very high iron levels, a single-echo approach should be adopted to reduce the minimum TE. Correction for liver fat content was not performed. The steatotis may lead to an underestimation of T_2^* values (34). However, steatosis is a rare finding in thalassemia major patients, so this aspect should not affect the results of this study. The last limitation was the absence of a calibration curve between T_2^* values at 3 T and iron concentration measured in iron-loaded animals.

In conclusion, the assessment of T_2^* values at 3 T seemed to be feasible, reproducible, and reliable to quantify iron burden in the whole left ventricle, in the mid-ventricular septum and in no heavy–moderate overloaded livers. At 3 T challenge was the segmental heart T_2^* analysis due to significantly higher T_2^* susceptibility artifacts and the detection of the patients with heavy–moderate liver iron burden. However, T_2^* measurements at higher fields seemed not to offer any advantages versus the lower fields.

ACKNOWLEDGMENTS

The authors thank the following colleagues from the Italian thalassemia centers involved in the MIOT network: A. Quarta (Ospedale A. Perrino, Brindisi), M. Capra (Ospedale "G. di Cristina," Palermo), D. D'Ascola (A.O. Bianchi-Melacrino-Morelli, Reggio Calabria), A. Filosa (Ospedale Cardarelli, Napoli), M. C. Putti (Università / Azienda Ospedaliera, Padova), A. Spasiano (Ospedale Cardarelli, Napoli), C. Borgna-Pignatti (Università di Ferrara, Ferrara), V. Caruso (P.O. "S. Luigi-Currò" - ARNAS Garibaldi, Catania), P. Cianciulli (Ospedale "Sant'Eugenio Papa," Roma), M. G. Batzella (Ospedale San Gavino, San Gavino Monreale), and A. Carollo (Az. Osp.

"Sant'Antonio abate," Trapani). They thank the industrial sponsorships (Chiesi and GE Healthcare) that gave their "no-profit" support to the MIOT project and also thank all the radiologic technicians in our Laboratory for their cooperation, helpfulness and patience. They finally thank all patients and healthy subjects who underwent MRI for their double cooperation and Claudia Santarlasci for her skillful secretarial work.

REFERENCES

1. Maggio A, Capra M, Pepe A, Mancuso L, Cracolici E, Vitabile S, Rigano P, Cassara F, Midiri M. A critical review of non invasive procedures for the evaluation of body iron burden in thalassemia major patients. Pediatr Endocrinol Rev 2008;6 (suppl 1):193–203.
2. Borgna-Pignatti C, Rugolotto S, De Stefano P, Zhao H, Cappellini MD, Del Vecchio GC, Romeo MA, Forni GL, Gamberini MR, Ghilardi R, Piga A, Cnaan A. Survival and complications in patients with thalassemia major treated with transfusion and deferoxamine. Haematologica 2004;89:1187–1193.
3. Porter JB, Davis BA. Monitoring chelation therapy to achieve optimal outcome in the treatment of thalassaemia. Best Pract Res Clin Haematol 2002;15:329–368.
4. Modell B, Khan M, Darlison M, Westwood MA, Ingram D, Pennell DJ. Improved survival of thalassaemia major in the UK and relation to T2* cardiovascular magnetic resonance. J Cardiovasc Magn Reson 2008;10:42.
5. Cogliandro T, Derchi G, Mancuso L, Mayer MC, Pannone B, Pepe A, Pili M, Bina P, Cianciulli P, De Sanctis V, Maggio A. Guideline recommendations for heart complications in thalassemia major. J Cardiovasc Med (Hagerstown) 2008;9:515–525.
6. Tanner MA, He T, Westwood MA, Firmin DN, Pennell DJ. Multi-center validation of the transferability of the magnetic resonance T2* technique for the quantification of tissue iron. Haematologica 2006; 91:1388–1391.
7. Ramazzotti A, Pepe A, Positano V, Rossi G, De Marchi D, Brizi MG, Luciani A, Midiri M, Sallustio G, Valeri G, Caruso V, Centra M, Cianciulli P, De Sanctis V, Maggio A, Lombardi M. Multicenter validation of the magnetic resonance T2* technique for segmental and global quantification of myocardial iron. J Magn Reson Imaging 2009;30:62–68.
8. Yablonskiy DA, Haacke EM. Theory of NMR signal behavior in magnetically inhomogeneous tissues: the static dephasing regime. Magn Reson Med 1994;32:749–763.
9. Gati JS, Menon RS, Ugurbil K, Rutt BK. Experimental determination of the BOLD field strength dependence in vessels and tissue. Magn Reson Med 1997;38:296–302.
10. Tumkur S, Vu A, Li L, Prasad PV. Evaluation of intrarenal oxygenation at 3.0 T using 3-dimensional multiple gradient-recalled echo sequence. Invest Radiol 2006;41:181–184.
11. Storey P, Thompson AA, Carqueville CL, Wood JC, de Freitas RA, Rigsby CK. R2* imaging of transfusional iron burden at 3T and comparison with 1.5T. J Magn Reson Imaging 2007;25:540–547.
12. Guo H, Au WY, Cheung JS, Kim D, Jensen JH, Khong PL, Chan Q, Chan KC, Tosti C, Tang H, Brown TR, Lam WW, Ha SY, Brittenham GM, Wu EX. Myocardial T2 quantitation in patients with iron overload at 3 Tesla. J Magn Reson Imaging 2009;30:394–400.
13. Pepe A, Positano V, Santarelli F, Sorrentino F, Cracolici E, De Marchi D, Maggio A, Midiri M, Landini L, Lombardi M. Multislice multiecho T2* cardiovascular magnetic resonance for detection of the heterogeneous distribution of myocardial iron overload. J Magn Reson Imaging 2006;23:662–668.
14. Positano V, Pepe A, Santarelli MF, Scattini B, De Marchi D, Ramazzotti A, Forni G, Borgna-Pignatti C, Lai ME, Midiri M, Maggio A, Lombardi M, Landini L. Standardized T2* map of normal human heart in vivo to correct T2* segmental artefacts. NMR Biomed 2007; 20:578–590.
15. Positano V, Pepe A, Santarelli MF, Ramazzotti A, Meloni A, De Marchi D, Favilli B, Cracolici E, Midiri M, Spasiano A, Lombardi M, Landini L. Multislice multiecho T2* cardiac magnetic resonance for the detection of heterogeneous myocardial iron distribution in thalassaemia patients. NMR Biomed 2009;22:707–715.
16. Meloni A, Ramazzotti A, Positano V, Salvatori C, Mangione M, Marcheschi P, Favilli B, De Marchi D, Prato S, Pepe A, Sallustio G, Centra M, Santarelli MF, Lombardi M, Landini L. Evaluation of a web-based network for reproducible T2* MRI assessment of iron overload in thalassemia. Int J Med Inform 2009;78:503–512.
17. Meloni A, Luciani A, Positano V, De Marchi D, Valeri G, Restaino G, Cracolici E, Caruso V, Dell'amico MC, Favilli B, Lombardi M, Pepe A. Single region of interest versus multislice T2* MRI approach for the quantification of hepatic iron overload. J Magn Reson Imaging 2011;33:348–355.
18. Cerqueira MD, Weissman NJ, Dilsizian V, Jacobs AK, Kaul S, Laskey WK, Pennell DJ, Rumberger JA, Ryan T, Verani MS. Standardized myocardial segmentation and nomenclature for tomographic imaging of the heart: a statement for healthcare professionals from the Cardiac Imaging Committee of the Council on Clinical Cardiology of the American Heart Association. Circulation 2002;105:539–542.
19. Pepe A, Lombardi M, Positano V, Cracolici E, Capra M, Malizia R, Prossomariti L, de Marchi D, Midiri M, Maggio A. Evaluation of the efficacy of oral deferiprone in beta-thalassemia major by multislice multiecho T2*. Eur J Haematol 2006;76:183–192.
20. Positano V, Salani B, Pepe A, Santarelli MF, De Marchi D, Ramazzotti A, Favilli B, Cracolici E, Midiri M, Cianciulli P, Lombardi M, Landini L. Improved T2* assessment in liver iron overload by magnetic resonance imaging. Magn Reson Imaging 2009;27:188–197.
21. Reeder SB, Faranesh AZ, Boxerman JL, McVeigh ER. In vivo measurement of T*2 and field inhomogeneity maps in the human heart at 1.5 T. Magn Reson Med 1998;39:988–998.
22. Wood JC, Enriquez C, Ghugre N, Tyzka JM, Carson S, Nelson MD, Coates TD. MRI R2 and R2* mapping accurately estimates hepatic iron concentration in transfusion-dependent thalassemia and sickle cell disease patients. Blood 2005;106:1460–1465.
23. Anderson LJ, Holden S, Davis B, Prescott E, Charrier CC, Bunce NH, Firmin DN, Wonke B, Porter J, Walker JM, Pennell DJ. Cardiovascular T2-star (T2*) magnetic resonance for the early diagnosis of myocardial iron overload. Eur Heart J 2001;22:2171–2179.
24. Westwood M, Anderson LJ, Firmin DN, Gatehouse PD, Charrier CC, Wonke B, Pennell DJ. A single breath-hold multiecho T2* cardiovascular magnetic resonance technique for diagnosis of myocardial iron overload. J Magn Reson Imaging 2003;18:33–39.
25. Angelucci E, Brittenham GM, McLaren CE, Ripalti M, Baronciani D, Giardini C, Galimberti M, Polchi P, Lucarelli G. Hepatic iron concentration and total body iron stores in thalassemia major. N Engl J Med 2000;343:327–331.
26. Wood JC, Ghugre N. Magnetic resonance imaging assessment of excess iron in thalassemia, sickle cell disease and other iron overload diseases. Hemoglobin 2008;32:85–96.
27. O'Regan DP, Callaghan MF, Fitzpatrick J, Naoumova RP, Hajnal JV, Schmitz SA. Cardiac T2* and lipid measurement at 3.0 T-initial experience. Eur Radiol 2008;18:800–805.
28. Hernando D, Hines CD, Reeder SB. R2* estimation in the presence of fat and macroscopic B0 field variations. In: Proceedings of International Society for Magnetic Resonance in Medicine, Montreal, Vol. 19; 2011. p 2691.
29. Olson LJ, Edwards WD, McCall JT, Ilstrup DM, Gersh BJ. Cardiac iron deposition in idiopathic hemochromatosis: histologic and analytic assessment of 14 hearts from autopsy. J Am Coll Cardiol 1987; 10:1239–1243.
30. Ambu R, Crisponi G, Sciot R, Van Eyken P, Parodo G, Iannelli S, Marongiu F, Silvagni R, Nurchi V, Costa V, et al. Uneven hepatic iron and phosphorus distribution in beta-thalassemia. J Hepatol 1995;23:544–549.
31. Wood JC, Otto-Duessel M, Aguilar M, Nick H, Nelson MD, Coates TD, Pollack H, Moats R. Cardiac iron determines cardiac T2*, T2, and T1 in the gerbil model of iron cardiomyopathy. Circulation 2005;112:535–543.
32. Ghugre NR, Storey P, Rigsby CK, Thompson AA, Carqueville CL, Coates TD, Wood JC. Multi-field behavior of Relaxivity in an iron-rich environment. In: Proceedings of International Society for Magnetic Resonance in Medicine, Toronto, Vol. 16; 2008. p 644.
33. Positano V, Meloni A, Pepe A, Santarelli M, Marchi D, Menichetti L, Dell'Amico C, Favilli B, Milanesi M, Valeri G, Natale L, Tassi C, Casini T, Landini L, Lombardi M. Cramer-Rao lower bounds for precision in T2* assessment for myocardial iron overload measurements by T2* multi-echo CMR. J Cardiovasc Magn Reson 2010;12v(suppl 1):P275.
34. Reeder SB, Bice EK, Yu H, Hernando D, Pineda AR. On the performance of T(2)* correction methods for quantification of hepatic fat content. Magn Reson Med, in press; DOI 10.1002/mrm.23016.